Published in final edited form as:

*Nature*. 2016 April 21; 532(7599): 334–339. doi:10.1038/nature17629.

# X-ray structures and mechanism of the human serotonin transporter

**Jonathan A. Coleman**[a], **Evan M. Green**[a,1], and **Eric Gouaux**[a,b]

[a]Vollum Institute, Oregon Health & Science University, Portland, Oregon 97239, USA

[b]Howard Hughes Medical Institute, Oregon Health & Science University, Portland, Oregon 97239, USA

## Abstract

The serotonin transporter (SERT) terminates serotonergic signaling through the sodium and chloride dependent reuptake of neurotransmitter into presynaptic neurons. SERT is a target for antidepressant and psychostimulant drugs, which block reuptake and prolong neurotransmitter signaling. Here we report x-ray crystallographic structures of human SERT at 3.15 Å resolution bound to the antidepressants (*S*)-citalopram or paroxetine. Antidepressants lock SERT in an outward-open conformation by lodging in the central binding site, located between transmembrane helices 1, 3, 6, 8, and 10, directly blocking serotonin binding. We further identify the location of an allosteric site in the complex as residing at the periphery of the extracellular vestibule, interposed between extracellular loops 4 and 6 and TMs 1, 6, 10, and 11. Occupancy of the allosteric site sterically hinders ligand unbinding from the central site, providing an explanation for the action of (*S*)-citalopram as an allosteric ligand. These structures define the mechanism of antidepressant action in SERT and provide blueprints for future drug design.

Serotonin (5-hydroxytryptamine or 5-HT) modulates the activity of the central nervous system as well as processes throughout the body ranging from cardiovascular function to digestion, body temperature, endocrinology and reproduction(1). Discovered in the late 1940s as a signalling molecule, serotonin increases vasoconstriction after blood clotting, that is, serum-tone(2). In the brain, the raphe nuclei synthesize serotonin from tryptophan, and distribute serotonin via long projections that reach nearly every major brain region. Serotonin is released into the synaptic cleft between neurons, where it diffuses to activate serotonin receptors, a group of G-protein-coupled receptors and ligand-gated ion channels



Correspondence and requests for materials should be addressed to E.G. (gouauxe@ohsu.edu).

[1]Present address: Graduate Group in Biophysics, University of California, San Francisco, San Francisco, California 94158, USA.

**AUTHOR CONTRIBUTIONS**

J.A.C., E.M.G. and E.G. designed the project. E.M.G. and J.A.C. developed thermostable constructs for crystallization. J.A.C. performed protein purification, crystallography and biochemical analysis. J.A.C., E.M.G. and E.G. wrote the manuscript.

The coordinates for the ts3 paroxetine, ts2 paroxetine, ts3 S-citalopram, ts3 S-citalopram (soaked), ts3 bromocitalopram, ts3 bromocitalopram (soaked), and 8B6 Fab structures have been deposited in the Protein Data Bank under the accession codes 5I6X, 5I6Z, 5I71, 5I73, 5I74, 5I75, 5I66, respectively.

The authors declare no competing financial interests. Readers are welcome to comment on the online version of the paper.

that participate in both excitatory and inhibitory neurotransmission and modulate the release of many neurotransmitters and hormones. Thus, serotonergic signalling influences neurological processes including sleep, mood, cognition, pain, hunger and aggression behaviours. The discovery that serotonin reuptake into nerve terminals is inhibited by the tricyclic antidepressant imipramine in a manner similar to norepinephrine (also known as noradrenaline) reuptake provided an initial clue that transport occurs by a related reuptake system(3–5). Prozac was introduced as one of the first selective serotonin reuptake inhibitors (SSRIs) for the treatment of depression and, subsequently, the serotonin transporter gene (SERT, also known as SLC6A4) was cloned and proven to be the target of SSRIs(6,7).

SERT is a member of the neurotransmitter sodium symporter (NSS) family of transporters, which also includes the dopamine (DAT) and norepinephrine (NET) transporters. NSSs are responsible for the sodium and chloride dependent reuptake of neurotransmitters, thus terminating signaling of the biogenic amines[8,9]. The unbinding of inhibitors can be further modulated by serotonin(10) and antidepressants(11) acting at an allosteric site. Several neurological conditions are associated with NSS dysregulation including major depression, anxiety disorder, attention deficit hyperactivity disorder, epilepsy, and Parkinson's disease[8,9,12]. Pharmacological modulation of NSS function through the use of therapeutic drugs such as tricyclic antidepressants and SSRIs has been used to treat many psychiatric disorders[13]. Illicit drugs such as cocaine and methamphetamines block neurotransmitter reuptake and are commonly abused psychostimulants, diminishing the well-being of users and constituting a tremendous socioeconomic burden.

Knowledge of NSS structure has been guided, in part, by experiments on the bacterial ortholog LeuT, as well as by studies of the *Drosophila* DAT (dDAT). This previous work has shown that the NSS family of transporters contain an inverted-topological repeat of transmembrane helices (TMs) 1–5 and 6–10, a 'central' or primary binding site for substrate and ions approximately halfway across the membrane-spanning region of the transporters[14–18] and, in the outward-open conformation, a large extracellular vestibule. Recently, structures of the invertebrate dDAT have provided insight into NSS pharmacology[19–21]. Nevertheless, these studies fall short of defining the structural determinants responsible for the markedly diverse pharmacological profiles of NSSs, the allosteric mechanism of human SERT, and important characteristics of human transporters. Here we present structures of the human serotonin transporter in complex with two of the most widely prescribed antidepressants: (*S*)-citalopram and paroxetine. Structures of SERT illuminate the molecular features of SSRI inhibition and allosteric regulation as well as unexpected structural elements not present in transporters previously studied.

## Thermostable SERT-Fab complex

Wild-type human SERT[22] is unstable in detergent micelles and refractory to crystallization. We thus screened a panel of SERT mutants for enhanced thermostability using a high throughput ligand binding assay[23], and by fluorescence-detection size exclusion chromatography[24]. Two thermostabilizing mutations, I291A and T439S, were introduced into SERT, yielding the ts2 construct, stable in short-chain detergents. Using transporter protein isolated from baculovirus-transduced mammalian cells[25], together with a

recombinant anti-SERT Fab, we obtained small crystals of a ts2-Fab-paroxetine complex which diffracted X-rays to 4.5 Å resolution. To improve crystal order, we included a third thermostabilizing mutation (Y110A), yielding the ts3 construct, which further improved stability and produced crystals of the Fab complex with either (*S*)-citalopram or paroxetine which diffracted X-rays to 3.15 Å resolution (Extended Data Tables 1–2). Whereas the wild-type transporter exhibits serotonin transport with a $K_M$ of 1.9 ± 0.3 μM and a $V_{max}$ of 23 ± 1 pmol $min^{-1}$, similar to reported values[8], ts2 has a $K_M$ of 4.5 ± 0.6 μM and $V_{max}$ of 21 ± 5 pmol $min^{-1}$ (Fig. 1a). No detectable transport activity was found for ts3.

## Architecture of human SERT

The structure of the human serotonin transporter bound to (*S*)-citalopram or paroxetine exhibits an outward-open conformation with the antidepressant drug bound to the central site, halfway across the membrane and wedged into a cavity made up of residues from TMs 1, 3, 6, 8, and 10 (Fig. 1b,c). A second (*S*)-citalopram molecule was found in the allosteric site, within the extracellular vestibule of the (*S*)-citalopram cocrystal structure, approximately 13 Å from the central site. Akin to dDAT and LeuT, SERT has 12 transmembrane spanning helices with TMs 1–5 and 6–10 related by a pseudo-2-fold axis (Extended Data Fig. 1)[14,16,20,21]. The ts2 and ts3 transporters superimpose well (Extended Data Table 3), demonstrating that the additional mutation of the ts3 construct does not substantially perturb the functionally active ts2 transporter structure (Extended Data Fig. 2a). TMs 1 and 6 adopt short regions of non helical conformation as they skirt the central ligand site and contribute residues which bind inhibitors as well as coordinate $Na^+$ and $Cl^-$ ions. The conformation of TMs 1 and 6 are incompatible with formation of an occluded state, suggesting that the antidepressant molecules have locked the transporter in an outward-open conformation, similar to the inhibitor-bound outward-open conformations of dDAT and LeuT (Extended Data Table 3) [14,16,19,21,26].

The extracellular surface of SERT is largely composed of EL2, EL4, and EL6, with EL2 ‘combed-over’ the extracellular surface and providing 3376 $Å^2$ of solvent accessible surface area. A conserved disulfide bridge is formed between Cys200 and Cys209 in EL2[27]. EL2 is predicted to contain two *N*-linked glycosylation sites, Asn208 and Asn217[28], and electron density for a *N*-acetylglucosamine moiety was found linked to Asn208; weak density was also found near Asn217. Similar to dDAT, the intracellular surface of the transporter is capped by IL5, IL1, and the C-terminal helix. Unlike LeuT, yet reminiscent of dDAT, TM12 has a pronounced kink halfway across the membrane. There is a cholesterol hemisuccinate (CHS) molecule bound near TM12a.

The crystal lattice packing between two SERT molecules occurs at the kink in TM12, which also overlaps with a 2-fold crystallographic axis of symmetry (Extended Data Fig. 2c), thus generating an apparent SERT ‘dimer’. Experiments suggest that SERT is an oligomer in the membrane[29]. However, in detergent SERT is a monomer and we suggest that the SERT ‘dimer’ observed in this crystal form is unlikely to exist in a membrane bilayer because the predicted membrane spanning regions of each protomer are not aligned with one another. Because the electron density for the Fab constant domain was poor, we also solved the structure of Fab at 1.6 Å resolution to facilitate model building and refinement (Extended

Data Fig. 2f, Extended Data Table 1). The Fab binds to a large extracellular surface consisting of EL2 and EL4 in a symmetry related SERT, and this interface is further stabilized by interactions of EL2-EL2 and Fab-EL2 in the asymmetric unit (Extended Data Fig. 2d,e).

The structure of SERT shows that amino acid changes due to single nucleotide polymorphisms and mutations associated with psychiatric disorders are distributed throughout the structure (Extended Data Fig. 2b). Interestingly most of the altered residues face solvent or lipid[12], thus rendering their effect on SERT structure and function obscure. P339L, however, is located in the non helical region of TM6 neighboring the ligand binding site and, not surprisingly, this variant exhibits diminished transport activity. By contrast, other disease associated mutations and polymorphisms, including mutations at Ile425 in TM8, K201N in EL2[30] and S293F and L362M in TMs 5 and 7 enhance serotonin transport, respectively. Another class of mutations, such as Phe465 in TM9 and L550V in TM11, probably destabilize the transporter or, as in the case of the K605N substitution in the C-terminal helix, render the transporter insensitive to protein kinase G regulation. With the establishment of SERT structural analysis, together with SERT expression and purification, one can now determine more precisely how these mutations alter the structure and activity of SERT.

## Antidepressant bound at the central site

To probe the capacity of the ts2 and ts3 SERT constructs to bind antidepressants, we carried out binding studies using [$^3$H]-(*R/S*)-citalopram and [$^3$H]-paroxetine (Fig. 2a,b). (*R/S*)-citalopram binds with $K_D$ values of 2.1 ± 0.1, 1.9 ± 0.3, and 2.9 ± 0.5 nM to the wild-type, ts2, and ts3 variants[31], whereas paroxetine exhibits a $K_D$ of 0.08 ± 0.03, 0.17 ± 0.03, and 0.10 ± 0.02 nM for wild-type, ts2, and ts3 constructs[31], respectively.

We next investigated the structure of the antidepressant binding site in the paroxetine and (*S*)-citalopram complexes by dividing the site into subsites A, B, and C[15] (Fig. 2c–e). Multi-crystal averaging of three (*S*)-citalopram data sets resulted in electron density maps that supported placement of the cyanophtalane group in subsite C and the fluorophenyl in subsite B, in harmony with detailed mutagenesis and ligand-binding studies[32] (Fig. 2c). Nevertheless, because of the limited resolution of the diffraction data, we wanted to ensure that we had positioned (*S*)-citalopram correctly. To do this, we crystallized SERT with a bromine derivative of citalopram, (*R*/*S*)-1-[3-(dimethylamino)propyl]-1-(4-bromophenyl)-1,3-dihydroisobenzofuran-5-carbonitrile, where the 4-fluoro group is replaced with a bromine atom (Br-citalopram). Upon analysis of the resulting anomalous difference Fourier map, we found a strong anomalous signal (> 9σ) in subsite B, corresponding to the predicted position of the bromine atom of the bromo citalopram derivative and, by extension, the fluorine atom of (*S*)-citalopram (Fig. 2d). These data are consistent with the fluorophenyl group of (*S*)-citalopram occupying subsite B. The non-therapeutic *R*-enantiomer of citalopram has significantly weaker affinity for SERT, perhaps because the aromatic substituents swap subsites, relative to the *S*-enantiomer[33]. Inspection of $F_o$-$F_c$ omit electron density maps allowed placement of paroxetine in the central binding site with the benzodioxol and fluorophenyl groups in subsites B and C (Fig. 2e). It is noteworthy that the

chemically equivalent fluorophenyl groups of (*S*)-citalopram and paroxetine are positioned in different subsites.

The amine groups of (*S*)-citalopram and paroxetine occupy subsite A and interact with the carboxylate of the conserved Asp98[34] at a distance of 4.1 and 3.1 Å (Fig. 2f,g), perhaps explaining, in part, why paroxetine has a higher affinity for SERT in comparison to (*S*)-citalopram. Tyr95 localizes 4.2 and 5.3 Å beneath the amine groups of (*S*)-citalopram and paroxetine, forming a cation-π interaction crucial for citalopram and mazindol potency[35]. Tyr95 may also form a hydrogen bond with the oxygen of (*S*)-citalopram. Ser336 partners in an interaction network with ligands and ions by participating in $Na^+$ and $Cl^-$ coordination, ions which are essential for ligand binding and substrate transport[36–38].

Subsite B is particularly important for high affinity antidepressant interaction as evidenced by mutations that influence citalopram binding[32,39]. Tyr176 engages in hydrophobic interactions with the fluorophenyl and benzodioxol groups of (*S*)-citalopram and paroxetine while also hydrogen bonding with Asp98. Ile172, and Phe341 define a non-polar ridge that cradles the hydrophobic groups of the drugs, and inhibitor binding is weakened upon mutation of these residues[32,40]. Phe341 in SERT, which is equivalent to Phe325 in dDAT, has swung “downward” by nearly 40° and forms an aromatic interaction with the “face” of the cyanophtalane of (*S*)-citalopram and with the “edge” of the fluorophenyl group of paroxetine (Extended Data Fig. 3a–b). Ser439, Leu443, Ala169, and Ala173 define a cavity which is more hydrophobic in SERT in comparison to the equivalent cavity in dDAT, and into which the fluorine and dioxol ring groups of (*S*)-citalopram and paroxetine are inserted (Extended Data Fig. 3c). The fluorophenyl group of (*S*)-citalopram is positioned 1.5 Å deeper into this space compared with the benzodioxol of paroxetine (Extended Data Fig. 3b).

The fluorophenyl group of paroxetine stacks parallel to the ring of Phe335 in subsite C. In contrast, for (*S*)-citalopram, the cyanophtalane forms an edge-to-face aromatic interaction. Phe335 defines the extracellular gate, and TMs 1 and 6 are strikingly different when comparing SERT to dDAT bound to a substrate analog[19] (Extended Data Table 3), showing that (*S*)-citalopram and paroxetine “prop” TM6 in an outward-open conformation. Val501 and Thr497 form a mixed non polar/polar surface into which the fluoro and cyano groups of paroxetine and (*S*)-citalopram are found. In the case of (*S*)-citalopram, the cyano group is inserted 2.1 Å further into subsite C and the hydroxyl group of Thr497 is positioned 1.7 Å away from its position in the paroxetine state (Extended Data Fig. 3b). In accord with the SERT-citalopram x-ray structure, a modest increase in citalopram affinity is observed for the T497A mutant[39], which would allow additional space for the cyano group.

## Ion-binding sites

$Na^+$ and $Cl^-$ ions, which are essential for substrate transport and SSRI binding[41], could be identified with electron densities > 3σ in $F_o$-$F_c$ ‘omit’ maps (Extended Data Fig. 4), at positions similar to those found in dDAT (Extended Data Table 4). The Na1 site is made up of residues contributed from TMs 1, 6, and 7 and the ion is coordinated by Ala96, Asn101, Ser336, and Asn368. Whereas Na1 is coordinated, in part, by a water molecule in dDAT,

which in turn is hydrogen-bonded to Asp46, in SERT there is not sufficient density to place water at a similar position. The chloride ion is coordinated by Tyr121, Gln332, Ser336, and Ser372 from TMs 2, 6, and 7 with a mean coordination distance of 3.1 Å. Strong density for Na2 could be seen in the (*S*)-citalopram structure with the ion coordinated by Gly94, Val97, Leu434, Asp437, and Ser438 from TMs 1 and 8. Placing ions in the omit densities led to a loss in $F_o$-$F_c$ density and the *B*-values of the ions match the values of surrounding residues. The mean coordination distance (2.4 Å) corresponds to known coordinate distances for sodium[42]. Only weak density for Na2 could be seen in the paroxetine structure, while in the (*S*)-citalopram complex the density for $Cl^-$ was weak, perhaps reflecting the overall weaker density in these regions rather than a *bona fide* difference in occupancy.

## Extracellular and intracellular gates

The SERT SSRI complexes adopt an outward open conformation that exposes the cone-shape extracellular vestibule to aqueous solution, providing a pathway for substrates, inhibitors, and ions to reach the central binding site, approximately halfway across the membrane bilayer. As in LeuT, the extracellular vestibule harbors residues that form the extracellular gate, and is lined by TMs 1b and 6a, as well as extracellular regions of TMs 3, 8, 10, and 11, together with EL6 and the 'tip' of EL4. The mixed polar and non polar character of the extracellular vestibule provides low affinity binding sites for small molecules, similar to LeuT, and in SERT we find electron density attributed to a second (*S*)-citalopram molecule in the (*S*)-citalopram cocrystal structure and a maltose detergent head group in the paroxetine complex within the extracellular vestibule. (Fig. 3a,b) [14,43–45].

At the base of the vestibule is the extracellular gate, and near the cytoplasmic face of SERT is the intracellular gate (Extended Data Fig. 5a,b). In SERT, Tyr176 and Phe335 define the lower portion of the extracellular gate and are separated by a distance of 10 Å, thus providing open access to the extracellular vestibule. In comparison to the extracellular gate of dDAT, the equivalent region in SERT exhibits significant structural changes: Tyr176 and Asp98 are separated by 4.0 Å and TM10 is closer to TM1b, bringing Glu494 and Arg104 within 4.8 Å and thus the central site can only be accessed through the extracellular vestibule. The intracellular gate of SERT is closed, similar to the outward facing conformations of dDAT and LeuT, thus precluding direct access from the central ligand binding site to the intracellular solution (Fig. 3, Extended Data Fig. 5b).

## Allosteric site

To determine if the off-rate of inhibitor from the central site is modulated by a ligand binding to an allosteric site in the ts3 construct, we measured the dissociation of [$^3$H](*R/S*)-citalopram from the central site in the presence of saturating concentrations of cold (*S*)-citalopram. As shown in previous studies, micromolar concentrations of (*S*)-citalopram, serotonin, and other ligands slow dissociation from the central site[10,11]. For ts3, 100 μM (*S*)-citalopram decreased the first order rate of [$^3$H](*R/S*)-citalopram dissociation by nearly 10-fold compared to buffer alone (0.0032 ± 0.0007 *vs.* 0.025 ± 0.002 $min^{-1}$) (Fig. 4a), with the wild-type and ts2 transporters exhibiting similar effects (wild-type: 0.004 ± 0.001 *vs.* 0.035

± 0.004; ts2: 0.0028 ± 0.001 *vs.* 0.08 ±0.03 $min^{-1}$), thus showing that allosteric modulation of ligand unbinding is intact in the ts2 and t3 constructs.

The allosteric binding site of (*S*)-citalopram is defined by residues in TMs 1b, 6a, 10, and 11, and in EL4 and EL6 (Fig. 4b, Extended Data Fig. 5c) with prominent electron density (>5 σ in $F_o$-$F_c$ omit maps) present in this region for crystals soaked with (*S*)-citalopram. Interestingly, mutagenesis of residues proximal to the allosteric site has been reported to severely alter allosteric potency[46] yet the physiological role of this site is not well established[47]. Residues of the extracellular gate, Glu494 and Arg104, are located 4.1 and 4.8 Å from the aminopropyl group, while Asp328 is 6.8 Å away. Arg104 is also located 3.6 Å from the cyanophtalene ring and probably participates in a cation-π interaction, while the cyano group of the phtalane ring is 3.1 Å from the side chain amide of Gln332. Ala331 forms a non-polar groove into which the ring system of S-citalopram is buttressed. Phe556 is 3.5 Å from the fluorophenyl group and participates in aromatic interactions while a proline repeat (Pro560-Pro561) in EL6 demarcates the upper portion of the allosteric site, 6.6 Å from the fluorophenyl entity.

To confirm the identity of the ligand bound to the allosteric site, we soaked crystals with Br-citalopram. A strong anomalous signal (> 5σ) corresponding to bromine was detected in anomalous difference electron density maps, confirming the position and pose of citalopram in the allosteric site (Fig. 4c). However, there was not sufficient electron density to place the aminopropyl group of Br-citalopram and thus we excluded it from the structure.

In the paroxetine complex, we found electron density for a possible maltose entity, presumably derived from a detergent molecule. (Extended Data Fig. S5d) occupying a position in the extracellular vestibule that partially overlaps with (*S*)-citalopram bound in the allosteric site (Fig. 4d). Upon analysis of the allosteric site of the (*S*)-citalopram and paroxetine complexes we note considerable plasticity, presumably due to the nature of the bound molecule. Relative to the (*S*)-citalopram-bound allosteric site, in the paroxetine structure Phe556 moves “downward” toward TM6a, to a position underneath the maltose. In addition, Arg104 moves 2 Å further into the allosteric site, while EL6 also moves 1.3 Å toward TM10, with the largest change occurring at Pro561. The malleability of the allosteric site opens the possibility that, depending upon the shape and size of the allosteric ligand, occupancy of the allosteric site might not necessarily abrogate transport activity. Indeed, it is conceivable that there could be a spectrum of small molecules that range from inhibiting to enhancing transport activity.

Comparison of the allosteric site of SERT with the equivalent region of dDAT shows how the SERT site is distinct from that of dDAT, even though SERT and dDAT are highly similar in structure within their cores around the central ligand binding site (TMs 1–8, Extended Data Table 3). Indeed, there are marked differences between SERT and dDAT for TMs 9–12 and the extracellular loops (Fig. 5a, Extended Data Table 3). EL2, centrally positioned within the extracellular domain, is longer in SERT than in dDAT and participates in extensive interactions with EL4 and EL6, which together sculpt a portion of the allosteric site (Fig. 5b,c). Moreover, when comparing human SERT, DAT and NET amino acid sequences, EL6 displays one of the highest regions of diversity, consistent with the

observation that allosteric ligands of SERT do not modulate DAT or NET. Furthermore, EL6 adopts a unique conformation not observed in dDAT because it extends more than 4 Å further toward EL2.

The conformation of TMs 9–12 also defines the allosteric site (Fig. 5d). Comparisons between dDAT and SERT illustrate that in SERT TM9 is shifted toward TM12, perhaps coordinated by contacts via EL5 and TM10, the latter of which contains a short stretch of π-helix near Glu494, a key residue of the extracellular gate. In SERT, TM11 extends further into the putative membrane environment in comparison to dDAT, thus providing a larger cavity for allosteric ligands, while TM12a splays inward to buttress TMs 10 and 11. Finally, interaction of cholesterol, which is known to modulate transport and ligand binding[48] together with other lipid molecules, may reinforce the conformation of TM12. Indeed, in SERT a CHS molecule stacks against Trp573 in a groove formed by Leu577, Ile576, and Ala580 and the extracellular portion of TM12a (Extended Data Fig. 6b), along with a presumed alkyl chain of a detergent molecule bound in a cavity composed of residues from TMs 10 and 12a (Extended Data Fig. 6c).

## Intracellular surface and C-terminal hinge

IL5 and the intracellular half of TM11 are highly similar to dDAT, while IL4 is partially unwound due to the insertion of Trp458 (Fig. 5d). The C-terminus of SERT mimics dDAT with a similar hinge and helix region (Fig. 5e). Glu615 is thought to form a salt bridge with Arg152 in IL1[49], but no side chain density is present which makes assignment of C-terminal register not possible. We hypothesize that the disorder of the C-terminus is due to dynamic properties, perhaps related to its importance in trafficking[50].

## Conclusion

The SERT - SSRI complexes capture the transporter in an inhibitor-bound, outward-open conformation, illustrating how the bulky ligands lodge in the central binding site, preventing substrate binding and transporter isomerization to occluded and inward open conformations. Extensive interactions throughout the central binding site explain, in large part, the selectivity of SSRIs. The allosteric site is poised ‘above’ the central site, within the ‘walls’ of the extracellular vestibule, directly obstructing ligand egress from the central site, thus explaining how allosteric ligands slow the off-rate of inhibitors bound to the central site (Fig. 6). Taken together, the structures of the human serotonin transporter shed fresh insight into antidepressant recognition and the molecular basis for allosteric modulation of inhibitor binding and of transporter activity, thus providing a platform to design small molecules targeting the central and allosteric binding sites.

## METHODS

### Protein constructs

The cDNA encoding the human wild-type SERT[22] was cloned into the BacMam vector[25] with a C-terminal GFP tag. For crystallization studies, the ts3 variant contained thermostabilizing mutations Y110A, I291A, T439S and mutation of surface-exposed

cysteines C554A, C580A, C622A, and was fused to a C-terminal GFP followed by twin Strep [TrpSerHisProGlnPheGluLys(GlyGlyGlySer)$_2$GlyGlySerAlaTrpSerHisProGlnPheGluLys], and His10 purification tags. The His10 tag was used in thermostability studies to capture SERT on copper scintillation beads[23] while the twin Strep tag was used for large-scale purification. Thrombin cleavage sites (LeuValProArgGlySer) were introduced in the N- and C-terminus after residues Gln76 and Thr618. The ts2 construct is identical to ts3 except that ts2 does not have the Y110A mutation. To raise the 8B6 antibody, residues 73–616 of wild-type SERT were cloned into BacMam with a C-terminal StrepII tag (TrpSerHisProGlnPheGluLys) and without GFP.

### Anti-hSERT antibody discovery and Fab expression

The 8B6 monoclonal antibody (mAb) against SERT was raised by Dan Cawley (Vaccine and Gene Therapy Institute; OHSU). StrepII tagged SERT was purified by Strep Tactin affinity as described subsequently in DDM with 1 μM paroxetine. Liposomes containing asolectin:cholesterol:lipid A:brain polar lipid (60:17:3:20) were prepared in TBS (20 mM Tris pH 8, 100 mM NaCl) at a concentration of 40 mg/ml$^{-1}$ by extrusion through 200 nm filters. Liposomes were saturated with 5 mM *n*-dodecyl-β-D-maltoside (DDM) and purified SERT was added to the detergent:lipid mixture. DDM was removed by three successive additions of 80 mg/ml biobeads. For the first two additions, the biobeads were incubated for 2 hrs; the final incubation was overnight. 10 μM paroxetine was added to the proteoliposomes after reconstitution. SERT knockout mice were purchased from the Jackson Laboratory (mouse stain: 008355) and immunized with ~30 μg of reconstituted SERT. Hybridoma cell lines were generated as described[51] and screened by fluorescence-detection size-exclusion chromatography (FSEC)[24] and western blotting to select antibodies which recognize tertiary epitopes. The 8B6 mAb was purified from hybridoma supernatants using 4-mercapto-ethyl-pyridine resin. Fab was purified from papain digested mAb by cation exchange chromatography and was stored in 20 mM Tris pH 8, 150 mM NaCl, 10% glycerol.

The sequences of the 8B6 Fab light and heavy chain genes were determined by standard techniques. The genes of the 8B6 Fab were cloned into a bicistronic insect cell expression vector, including a GP67 signal peptide. A thrombin cleavage site and 8His tag were fused to the C-terminus of residues 1–235 of the heavy chain. The 8B6 Fab was purified from SF9 supernatant by metal ion affinity chromatography followed by cation exchange chromatography.

### Transporter expression and purification

The hSERT constructs were expressed as C-terminal GFP fusions using baculovirus-mediated transduction of mammalian HEK-293S GnTI$^-$ cells, as previously described[25,52]. Cells were subsequently solubilized in 50 mM Tris pH 8, 150 mM NaCl containing 20 mM DDM, 2.5 mM cholesteryl hemisuccinate (CHS), 0.5 mM dithiothreitol (DTT) in the presence of 1 μM inhibitor (paroxetine, (*S*)-citalopram, or Br-citalopram). The lysate was passed over 10 ml of Strep Tactin resin, washed with 18 column volumes of 1 mM DDM, 0.2 mM CHS, 5% glycerol, 25 μM lipid (1-palmitoyl-2-oleoyl-sn-glycero-3-phosphocholine,

1-palmitoyl-2-oleoyl-sn-glycero-3-phosphoethanolamine, and 1-palmitoyl-2-oleoyl-sn-glycero-3-phosphoglycerol at a molar ratio of 1:1:1), and 1 μM ligand in TBS. SERT was eluted in the same buffer containing 5 mM desthiobiotin. The N- and C-terminus containing GFP and purification tags were removed by thrombin digestion and *N*-linked sugars were truncated using EndoH. SERT was mixed with recombinant 8B6 Fab at a 1:1.2 molar ratio. In the case of Br-citalopram complexed at the central site, Fab purified from hybridoma cells was used. The resulting complexes were further purified by size exclusion chromatography in TBS supplemented with 40 mM *n*-octyl β-D-maltoside, 0.5 mM CHS, 5% glycerol, 25 μM lipid, and 1 μM inhibitor. The purified SERT-8B6 complex was concentrated to 2 mg/ml$^{-1}$ and the transporter solution was spiked with 10 μM inhibitor and 1 μM 8B6 Fab, final concentrations, immediately prior to crystallization.

## Crystallization

The SERT-Fab complex and Fab crystals were grown by hanging drop vapor diffusion. For the ts3-Fab complex, crystals appeared after several days under conditions with a reservoir solution composed of 100 mM Tris pH 8.5, 25–125 mM KCl, 32.5–34% PEG 400, and 0.5% 6-aminohexanoic acid with either paroxetine or (*S*)-citalopram at ratio of 2 μl protein to 1 μl of reservoir solution. Crystals of ts3-Fab complex with Br-citalopram bound to the central site were grown with a reservoir solution composed of 100 mM Tris pH 8.5, 125 mM NaCl, 125 mM $MgCl_2$, and 33.4% PEG 400. 'Soaked' SERT-Fab crystals were prepared by addition of 5 mM ligand ((*S*)-citalopram or Br-citalopram) overnight to the crystals as indicated. For the ts2-Fab complex, crystals were grown using a reservoir solution containing 100 mM Tris pH 8, 250 mM LiCl, and 34.7% PEG 400 with paroxetine. All SERT-Fab crystals were grown at 4°C, reaching full size after 14 days, and were directly flash frozen in liquid nitrogen prior to X-ray diffraction data collection. The 8B6 Fab from hybridoma cells was crystallized in 100 mM HEPES pH 7.5, 300 mM $NH_4H_2PO_4$, and 22.5% pure PEG (0.3–0.8 kDa PEG, Microlytic) at 4°. Fab crystals were cryoprotected with 25% ethylene glycol prior to flash cooling in liquid nitrogen.

## Data collection and structure refinement

X-ray diffraction data sets were collected at the Advanced Photon Source (Argonne National Laboratory, beamline 24-IDC and 24-IDE) and at the Advanced Light Source (Lawrence Berkeley National Laboratory, beamline 5.0.2). X-ray data was processed using XDS[53]. Molecular replacement was carried out to solve the 8B6 structure using the constant and variable domains of a preexisting Fab structure (PDB code: 4LQF) as independent search models, followed by automated and manual model building and refinement using Phaser, Coot, Phenix AutoBuild, and Phenix Refine[54–56]. The SERT-Fab data was processed using the microdiffraction assembly method[57] where indicated. The SERT structure was solved by molecular replacement using a multi-model search in Phaser with a homology model built using the dDAT structure (PDB code: 4M48) and Modeller[58] and the constant and variable domains of the 8B6 Fab structure. Multiple rounds of refinement and manual model building were carried out using Phenix and Coot, respectively, until the models were refined to acceptable R-factors and stereochemistry.

### Radioligand binding and uptake assays

Ligand binding experiments were carried out by adding HEK293 membranes containing SERT to a final concentration of 2 nM in 1 ml of TBS with either [$^3$H]paroxetine 0.01–10 nM or [$^3$H](*R/S*)-citalopram 0.01–20 nM. Reactions were rotated at room temperature for 4 hours followed by filtering through a glass microfiber filter prewet with 0.4% polyethylenimine in TBS. Membranes were washed 3x with 4 ml of TBS followed by liquid scintillation counting. Data was fit to a single-site binding curve accounting for ligand depletion. For dissociation, 20 nM SERT in membranes was mixed with 40 nM [$^3$H](*R/S*)-citalopram in 10 µl; samples were diluted to 1 ml in TBS with 100 µM (*S*)-citalopram, or without ligand, followed by filtering. For uptake assays, ~$10^5$ HEK293 cells in 96-well Cytostar T plates were transfected with 0.2 µg of plasmid with Polyjet. After 24–36 hrs, cells were washed with 25 mM HEPES-Tris pH 7.0, 130 mM NaCl, 5.4 mM KCl, 1.2 mM $CaCl_2$, 1.2 mM $MgSO_4$, 1 mM ascorbic acid, and 5 mM glucose. For a control, 10 µM paroxetine was added. [$^{14}$C]5-hydroxytryptamine at concentrations of 0.02–40 µM was added and uptake was followed using a MicroBeta scintillation counter. Data was fit to a Michaelis-Menten equation.

## Extended Data

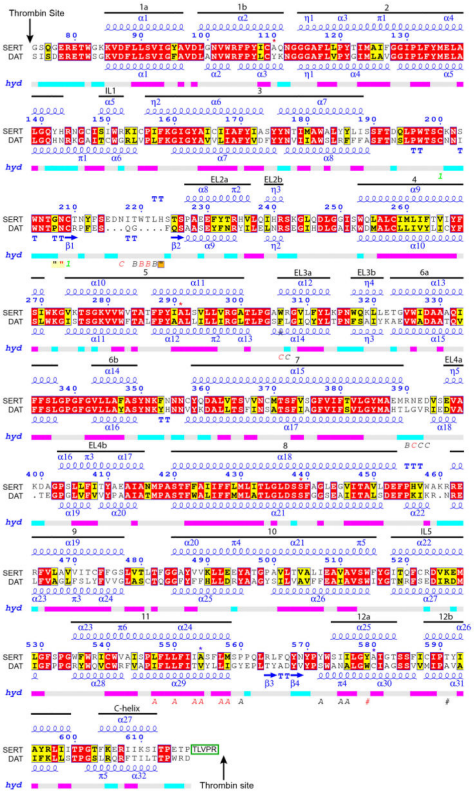


**Extended Data Figure 1. Construct design and secondary structure**

Thrombin digestion sites were introduced within the N- and C-terminal regions before Q76 and after T618. Mutations which were introduced to increase thermostability (Y110A, I291A, T439S) are indicated (red star). Surface exposed cysteines were mutated to alanine

(C554, C580) and indicated with a blue star. Residues which have no electron density are boxed in green. Secondary structure was analyzed using DSSP (http://swift.cmbi.ru.nl/gv/dssp/ ) and displayed using ENDScript (http://endscript.ibcp.fr/). Secondary structure elements are shown using the following symbols: α-helix (α), β-strand (β), π-helix (π), $3_{10}$ helix (η), β-turn (TT letters), α-turn (TTT letters). Locations of carbohydrate (red, “) and disulfide bonding cysteine (green digits) residues are also shown. *A–C* in italic means the residue has a crystallographic contact with a residue in Chain A–C. The ‘#’ symbol identifies a contact between two residues along the crystallographic 2-fold axis of symmetry. Contacts between transporter residues and small molecules in the range of 3.2–5.0 Å are also indicated (black, “). Hydropathy is calculated according to Kyte & Doolittle and shown with pink as hydrophobic (H > 1.5), cyan as hydrophilic (H < 1.5), and grey as intermediate. The secondary structure of the dopamine transporter (4M48) is shown for comparison.

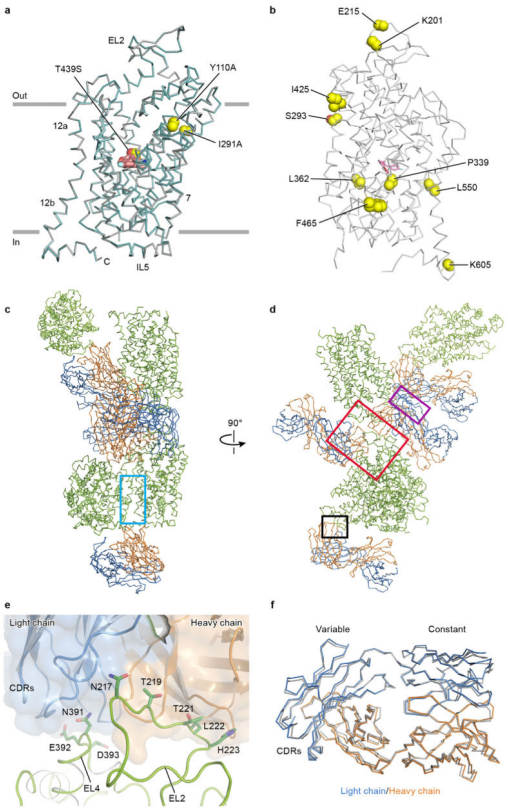


**Extended Data Figure 2. Comparison of the ts3 and ts2 structures, crystal packing and antibody structure**

**a,** Superposition of the ts2 (blue) and ts3 (grey) transporters, each in complex with paroxetine using all atoms (Extended Data Table 3). Paroxetine (pink sticks) and thermostabilizing mutations (yellow spheres). **b**, Position of amino acid changes due to single nucleotide polymorphisms and mutants associated with psychiatric disorders (yellow). Paroxetine is shown in pink. **c**, SERT is shown in green, Fab heavy chain (orange), light chain (blue). SERT molecules pack into the crystal lattice with SERT-SERT interface occurring along the kink of TM12 helices related by the crystallographic 2-fold axis (blue

box). **d**, Rotation by 90° reveals further lattice contacts. Red box shows interface between Fab, EL2, and EL4. We predict that this interface contains the high-affinity interaction of the Fab with EL2 and EL4. Also shown is a EL2-EL2 interaction between symmetry related molecules as well as a Fab-EL2 interface in the asymmetric unit. Purple box shows interface between Fab variable domains. Black box shows crystal contact between the C-terminal helix and the Fab constant domain. **e**, The binding site of the 8B6 Fab is made up of interactions of residues from EL2 and EL4 (sticks). **f**, Comparison of the high resolution Fab structure (grey) with SERT-bound Fab (Extended Data Table 3). The largest structural changes occur in the complementary determining regions (CDRs).

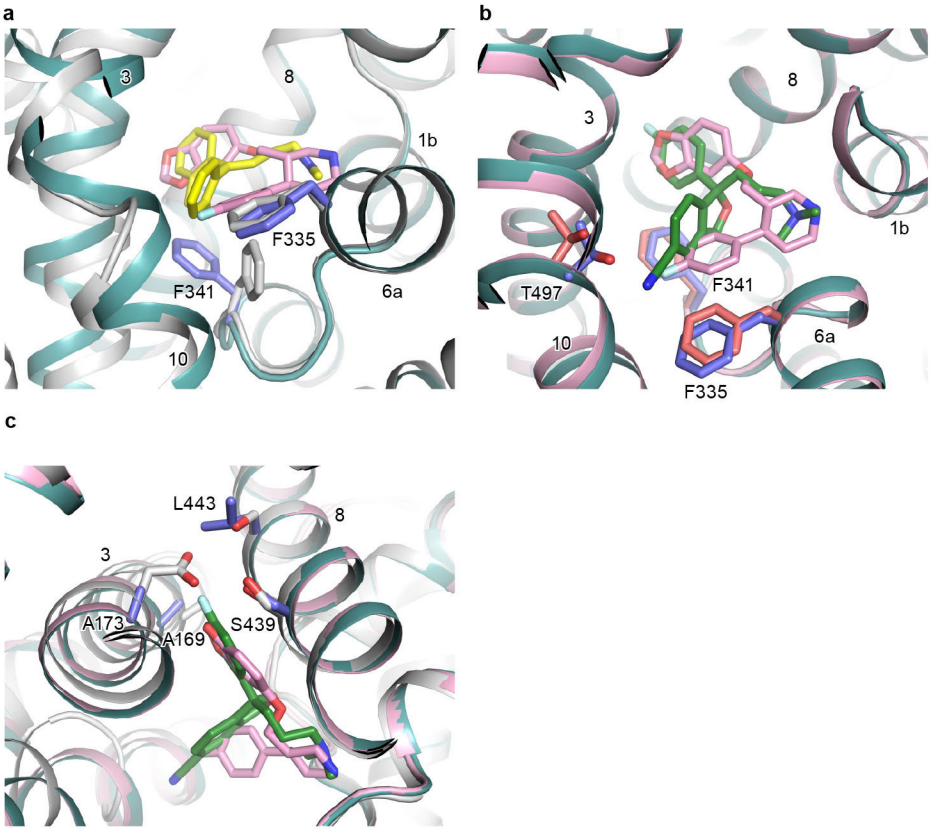


**Extended Data Figure 3. Comparison of ligand binding in SERT and in DAT**

**a**, Comparison of SERT bound to paroxetine with dDAT (4M48) bound to nortriptyline (yellow); superposition based on TMs 1–12. SERT is shown in blue and DAT in grey. **b**, Alignment of paroxetine (blue) and (*S*)-citalopram (pink) structures using all atoms in superposition (Extended Data Table 3). Residues interacting with the antidepressant molecules are shown as sticks. Paroxetine (pink) and (*S*)-citalopram (green) are shown as sticks. **c**, Insertion of benzodioxol and fluorophenyl groups of paroxetine and (*S*)-citalopram into a cavity in subsite B made up of L443, A169, A173, and S439. Note that Ser439 is equivalent to Thr439 in wild-type SERT. Equivalent residues in dDAT are shown in grey.

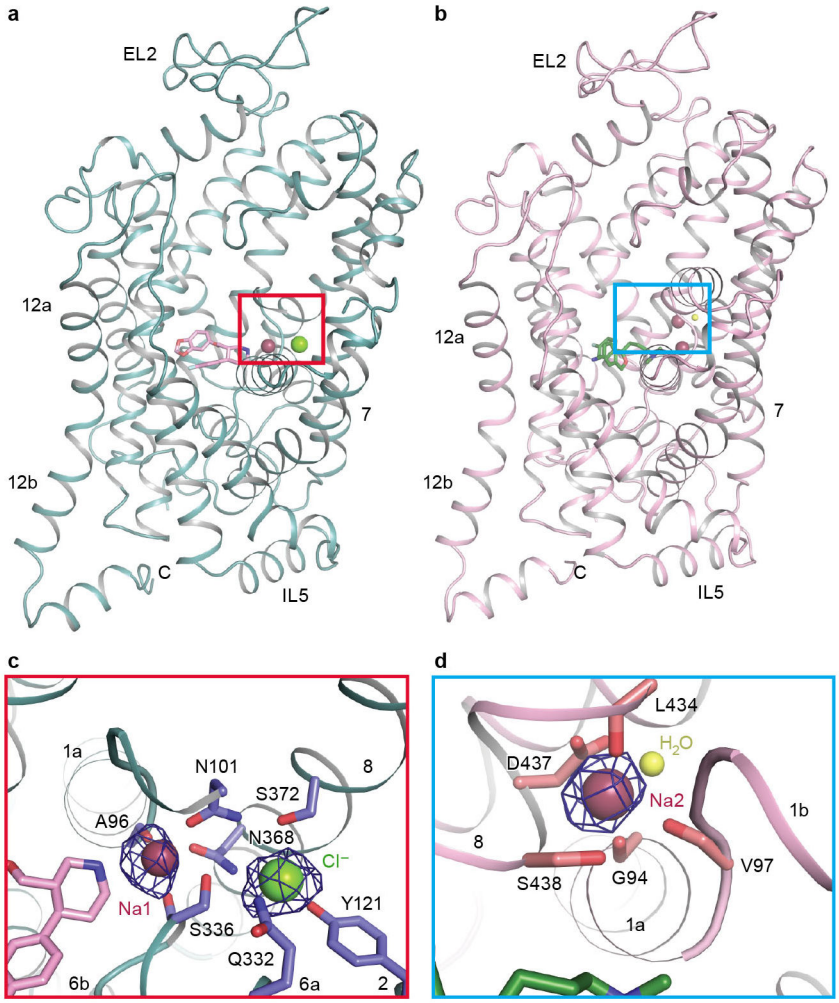


**Extended Data Figure 4. Ion binding sites**

**a**, Overall view of the Na1 and $Cl^-$ ion binding sites in the paroxetine bound transporter. $Na^+$ (salmon) and $Cl^-$ (green) are shown as spheres. Paroxetine is shown as pink sticks. **b**, Overall view of the (*S*)-citalopram bound transporter showing the Na2 binding site; (*S*)-citalopram (green sticks). **c**, Residues coordinating Na1 and $Cl^-$. Ion $F_o$-$F_c$ omit densities are shown at 2σ and 3σ for Na1 and $Cl^-$. **d**, Residues coordinating Na2. $F_o$-$F_c$ omit density is shown at 4σ. A water molecule is shown as a yellow sphere. Coordination distances are given in Extended Data Table 4.

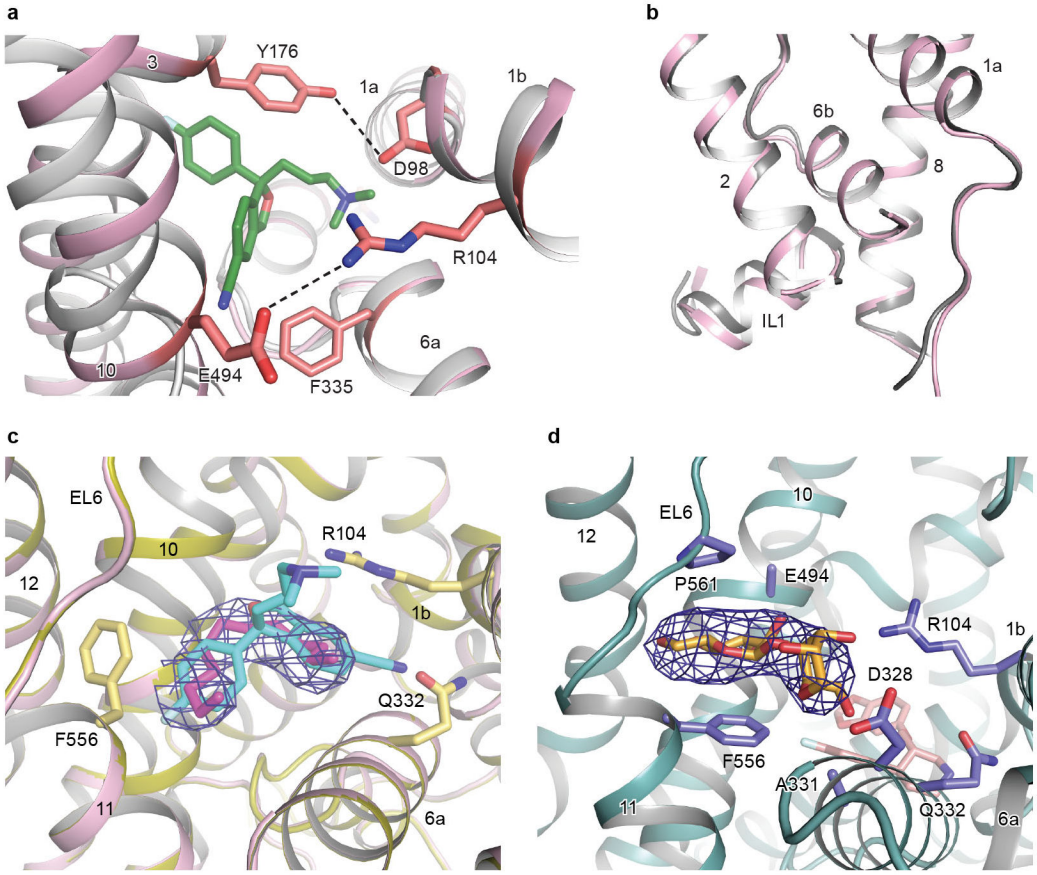


**Extended Data Figure 5. Extracellular and intracellular gates and the allosteric site of paroxetine and partially occupied (*S*)-citalopram**

**a**, The extracellular gate of the SERT-(*S*)-citalopram complex is shown, with (*S*)-citalopram bound to the central site. The width of the gate is depicted by the distances between Y176 and F335 (10.3 Å, CD1-CE2), D98 and Y176 (4.0 Å, OD2-OH), E494 and R104 (4.9 Å, OE1-NH1) dDAT (grey) is shown for comparison. **b**, Comparison of the intracellular gate of SERT (pink) *vs.* DAT (4M48, grey). Superpositions were made by alignment of TMs 1–12 of SERT with dDAT. **c**, The allosteric site containing fully occupied (*S*)-citalopram (pink) was superposed with the partially occupied structure (olive). The $F_o$-$F_c$ omit density (blue mesh) of the partially occupied structure is shown at 2σ. (*S*)-citalopram is shown in green sticks. A 12-carbon chain (magenta) was modeled into this density but could instead represent a partially occupied (*S*)-citalopram. The structure with partial (*S*)-citalopram occupancy at the allosteric site was derived from crystals grown in the presence of 10 μM ligand. Crystals with a higher occupancy at the allosteric site were soaked in a solution containing 5 mM (*S*)-citalopram prior to crystal cryo protection. **d**, The paroxetine-bound transporter contains a maltose detergent headgroup (orange) bound to the allosteric site. $F_o$-$F_c$ maltose omit density at 3σ.

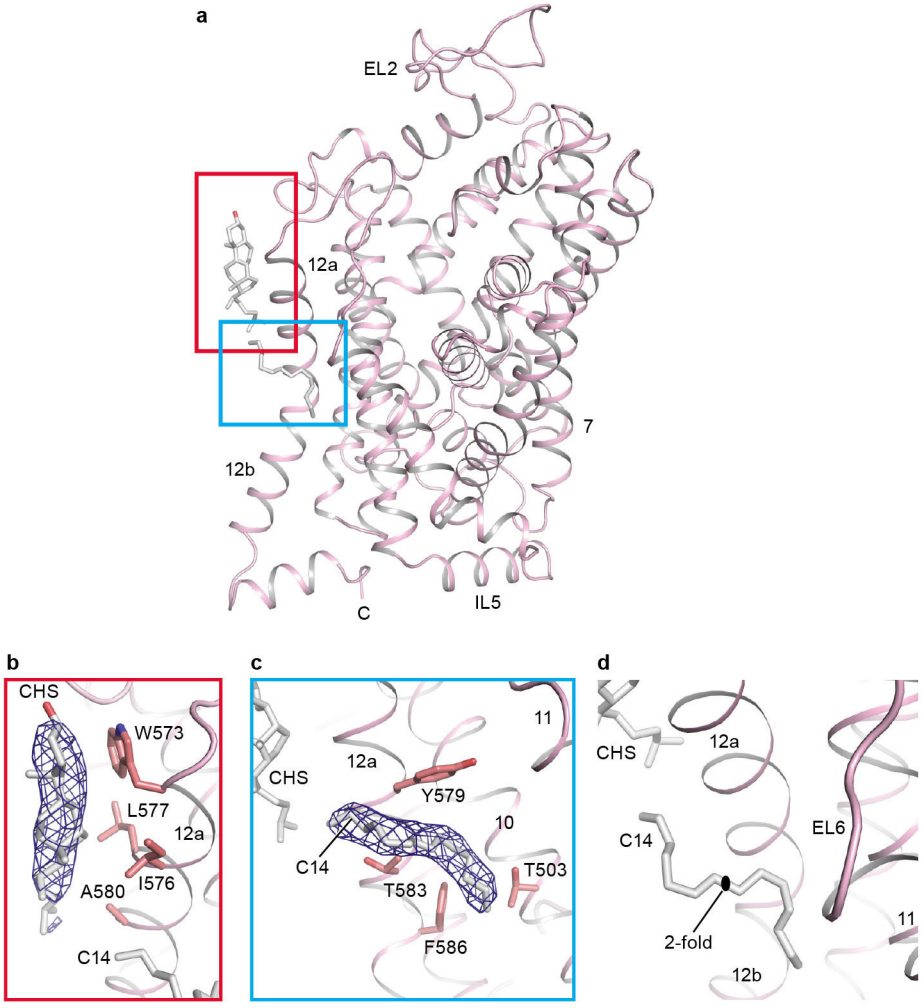


**Extended Data Figure 6. Cholesteryl hemisuccinate and tetradecane binding sites**

**a**, Overall view of the (*S*)-citalopram-bound structure showing cholesteryl hemisuccinate (CHS, red box) and tetradecane (C14, blue box). **b**, Zoomed view of the CHS binding site. Residues near CHS are shown as sticks. The $F_o$-$F_c$ omit density map is shown at 3σ. **c**, Binding of tetradecane. The $F_o$-$F_c$ omit density map is contoured at 4σ. **d**, Tetradecane was modeled on a 2-fold axis of symmetry with partial occupancy as a single molecule. Based on the density, it is unclear if this molecule represents the alkyl chain of a lipid, detergent, or a molecule of PEG.

## Extended Data Table 1

Data collection and refinement statistics.

| | Paroxetine ts3 * | Paroxetine ts2 † | (*S*)-citalopram ts3 ‡ | (*S*)-citalopram soaked ts3 § | 8B6 Fab ‖ |
|---|---|---|---|---|---|
| **Data collection** | APS24-IDE | ALS 5.0.2 | ALS 5.0.2 | ALS 5.0.2 | ALS 5.0.2 |
| Space group | $C222_1$ | $C222_1$ | $C222_1$ | $C222_1$ | $P4_32_12$ |

| | Paroxetine ts3 * | Paroxetine ts2 † | (*S*)-citalopram ts3 ‡ | (*S*)-citalopram soaked ts3 § | 8B6 Fab ‖ |
|---|---|---|---|---|---|
| Cell dimensions | | | | | |
| *a*, *b*, *c* (Å) | 129.2, 162.8, 140.4 | 129.8, 162.8, 140.1 | 129.7, 163.7, 140.6 | 129.9, 163.2, 140.5 | 81.6, 81.6, 142.2 |
| α, β, γ (°) | 90.0, 90.0, 90.0 | 90.0, 90.0, 90.0 | 90.0, 90.0, 90.0 | 90.0, 90.0, 90.0 | 90.0, 90.0, 90.0 |
| Wavelength | 0.979 | 1.000 | 1.000 | 0.978 | 1.000 |
| Resolution (Å) | 53.17–3.14 (3.25–3.14) ¶ | 40.50–4.53 (4.69–4.53) | 53.33–3.15 (3.26–3.15) | 47.68–3.24 (3.36–3.24) | 57.67–1.62 (1.68–1. |
| $R_{meas}$ | 12.9 (63.5) | 20.0 (>100) | 6.7 (57.4) | 8.3 (60.3) | 5.7 (>100) |
| $I/\sigma I$ | 15.20 (3.1) | 8.20 (0.63) | 15.27 (1.99) | 14.32 (2.27) | 18.9 (0.61) |
| Completeness (%) | 99.9 (100.0) | 99.4 (95.5) | 99.1 (98.9) | 99.0 (92.0) | 97.7 (76.6) |
| Redundancy | 17.7 (12.5) | 7.1 (5.9) | 5.5 (4.0) | 10.5 (6.6) | 6.7 (2.9) |
| $CC_{1/2}$ (%) | 99.9 (13.8) | 99.9 (24.5) | 99.9 (14.0) | 99.9 (11.0) | 99.9 (21.5) |
| **Refinement** | | | | | |
| Resolution (Å) | 53.17–3.14 | 40.50–4.53 | 53.33–3.15 | 47.68–3.24 | 57.67–1.62 |
| No. reflections | 26151 (2585) | 8837 (828) | 25995 (2577) | 23870 (2178) | 59809 (4634) |
| $R_{work}$/ $R_{free}$ | 23.8 (38.3) / 27.0 (41.9) | 28.0 (38.9) / 31.7 (37.1) | 24.0 (39.1) / 27.6 (40.0) | 23.5 (37.5) / 27.6 (38.0) | 17.8 (42.4) / 19.8 (44.6) |
| No. atoms | 7631 | 7544 | 7616 | 7633 | 3604 |
| Protein | 7526 | 7530 | 7515 | 7503 | 3302 |
| Ligand/ion | 104 | 14 | 100 | 129 | N/A |
| Water | 1 | 0 | 1 | 1 | 302 |
| B-factors | | | | | |
| Protein | 157.0 | 398.13 | 159.9 | 175.8 | 40.1 |
| Ligand/ion | 158.3 | 302.8 | 157.0 | 173.0 | N/A |
| Water | 133.5 | N/A | 103.3 | 145.0 | 43.0 |
| R.m.s deviations | | | | | |
| Bond lengths (Å) | 0.008 | 0.004 | 0.008 | 0.015 | 0.012 |
| Bond angles (°) | 0.80 | 0.93 | 1.026 | 1.085 | 1.15 |
| Ramachandran plot | | | | | |
| Favored (%) | 95.7 | 96.1 | 95.6 | 95.7 | 98.1 |
| Allowed (%) | 4.3 | 3.9 | 4.4 | 4.3 | 1.9 |
| Disallowed (%) | 0 | 0 | 0 | 0 | 0 |

* Six crystals were merged for the Paroxetine ts3 structure using microdiffraction assembly.

† A single crystal was used for the Paroxetine ts2 structure.

‡ A single crystal was used for the (*S*)-citalopram ts3 structure and processed by microdiffraction assembly.

§ Three crystals were merged for the (*S*)-citalopram soaked ts3 structure using microdiffraction assembly.

‖ A single crystal was used for the 8B6 Fab structure.

¶ Highest resolution shell is shown in parenthesis.

5% of reflections were used for calculation of $R_{free}$.

## Extended Data Table 2

Anomalous data collection and refinement statistics.

| | Br-citalopram ts3 * | Br-citalopram soaked ts3 † |
|---|---|---|
| **Data collection** | APS24-IDC | ALS 5.0.2 |
| Space group | $C222_1$ | $C222_1$ |
| Cell dimensions | | |
| *a, b, c* (Å) | 129.6, 164.0, 140.2 | 129.6, 163.4, 140.5 |
| *α, β, γ* (°) | 90.0, 90.0, 90.0 | 90.0, 90.0, 90.0 |
| Wavelength | 0.902 | 0.900 |
| Resolution (Å) | 101.7–3.40 (3.52– 3.40) ‡ | 82.29–3.49 (3.61–3.48) |
| $R_{meas}$ | 6.3 (58.2) | 8.8 (59.5) |
| $I/\sigma I$ | 17.60 (2.44) | 17.76 (2.52) |
| Completeness (%) | 99.9 (97.0) | 99.5 (95.3) |
| Redundancy | 10.7 (7.0) | 11.0 (6.7) |
| $CC_{1/2}$ (%) | 100.0 (23.2) | 99.9 (12.5) |
| **Refinement** | | |
| Resolution (Å) | 101.7–3.40 | 82.29–3.49 |
| No. reflections | 20919 (2004) | 19231 (1812) |
| $R_{work}/R_{free}$ | 26.7 (39.8)/28.3 (47.1) | 24.2 (35.5)/29.3 (36.5) |
| No. atoms | 7610 | 7610 |
| Protein | 7512 | 7497 |
| Ligand/ion | 98 | 113 |
| Water | 0 | 0 |
| B-factors | | |
| Protein | 221.04 | 180.0 |
| Ligand/ion | 172.9 | 143.9 |
| Water | N/A | N/A |
| R.m.s deviations | | |
| Bond lengths (Å) | 0.004 | 0.016 |
| Bond angles (°) | 0.933 | 0.927 |
| Ramachandran plot | | |
| Favored (%) | 95.8 | 95.5 |
| Allowed (%) | 4.2 | 4.5 |
| Disallowed (%) | 0 | 0 |

* A single crystal was used for the Br-citalopram ts3 structure and processed by microdiffraction assembly.

† A single crystal was used for the Br-citalopram soaked ts3 structure and processed by microdiffraction assembly.

‡ Highest resolution shell is shown in parenthesis.

5% of reflections were used for calculation of $R_{free}$.

## Extended Data Table 3

Superpositions of DAT, LeuT, ts2 SERT, and ts3 (*S*)-citalopram conformational states vs. ts3 SERT (paroxetine) and comparison of high resolution Fab *vs.* SERT-bound Fab (paroxetine).

| Structure | Rmsd (Å) / Cα # |
|---|---|
| SERT TM1-12 *vs.* DAT (comp. inh: nortriptyline; 4M48) | 0.7 / 272 |
| SERT TM1-12 *vs.* DAT (sub. analog: 3,4-dichlorophenethylamine; 4XPA) | 0.8 / 283 |
| SERT TM1,6 *vs.* DAT (comp. inh: nortriptyline; 4M48) | 0.4 / 50 |
| SERT TM1,6 *vs.* DAT (sub. analog: 3,4-dichlorophenethylamine; 4XPA) | 0.6 / 52 |
| SERT TM1-8 *vs.* DAT (comp. inh: nortriptyline; 4M48) | 0.5 / 200 |
| SERT TM9-12 *vs.* DAT (comp. inh: nortriptyline; 4M48) | 1.2 / 137 |
| SERT EL2, EL4, EL6 vs. DAT (comp. inh: nortriptyline; 4M48) | 1.2 / 80 |
| SERT TM1-12 *vs.* LeuT (sub. free; 3TT1) | 1.3 / 260 |
| SERT TM1-12 *vs.* LeuT (comp. inh: tryptophan; 3F3A) | 1.4 / 249 |
| SERT TM1-12 *vs.* LeuT (sub. bound: leucine; 2A65) | 1.7 / 285 |
| SERT TM1-12 *vs.* LeuT (inward-open; 3TT3) | 2.9 / 282 |
| ts3 (*S*)-citalopram SERT *vs.* ts3 paroxetine SERT | 0.3 / 489 |
| ts2 SERT *vs.* ts3 SERT | 0.1 / 514 |
| High resolution Fab *vs.* SERT-bound Fab | 0.8 / 414 |

Superpositions were done by overlapping the Cα atoms of DAT, LeuT, or SERT ts2 over Cα atoms of SERT ts3 (paroxetine) using PyMOL. An outlier rejection cutoff of 2.0 RMS was used for five iterative cycles to reject structural outliers during the fit.

## Extended Data Table 4

Ion-binding sites and coordination distances.

| Site | Coordinating group | Location | Distance* (Å) |
|---|---|---|---|
| Na1 † | Ala 96-CO- | TM1a | 2.3 |
| | Asn 101 Oδ1 | TM1b | 2.3 |
| | Ser 336 Oγ | TM6a | 2.5 |
| | Ser 336-CO | TM6a | 2.4 |
| | Asn 368 Oδ1 | TM7 | 2.6 |
| | mean distance | | 2.4 |
| $Cl^-$ † | Tyr 121 OH | TM2 | 2.6 |
| | Gln 332 Nε | TM6a | 3.1 |
| | Ser 336 Oγ | TM6a | 3.6 |
| | Ser 372 Oγ | TM7 | 3.0 |
| | mean distance | | 3.1 |
| Na2 ‡ | Gly 94-CO- | TM1a | 2.5 |
| | Val 97-CO- | TM1b | 2.4 |
| | Leu 434-CO- | TM8 | 2.3 |
| | Asp 437 Oδ1 | TM8 | 2.4 |
| | Ser 438 Oγ | TM8 | 2.5 |
| | mean distance | | 2.4 |

* Interatomic distance between coordinating atom of protein chain to the bound ion(s).

†Determined from the ts3 paroxetine bound structure.

‡Determined from the ts3 (*S*)-citalopram bound structure.

## Acknowledgments

We thank D. Cawley for generating monoclonal antibodies and Lundbeck for Br-citalopram. We thank A. Penmatsa and K. Wang for assistance with initial crystal screening. K. Dürr and W. Lü are thanked for help with Fab crystallization and structure refinement respectively, L. Vaskalis for assistance with figures, H. Owen for help with manuscript preparation and other Gouaux laboratory members for helpful discussions. We acknowledge the staff of the Berkeley Center for Structural Biology at the Advanced Light Source and the Northeastern Collaborative Access Team at the Advanced Photon Source for assistance with data collection. J.A.C has support from a Banting postdoctoral fellowship from the Canadian Institutes of Health Research. We are particularly grateful to Bernie and Jennifer LaCroute for their generous support, as well as for funding from the NIH (5R37MH070039). E. G. is an investigator of the Howard Hughes Medical Institute.

## References

1. Berger M, Gray JA, Roth BL. The expanded biology of serotonin. Annu Rev Med. 2009; 60:355–366. [PubMed: 19630576]
2. Rapport MM, Green AA, Page IH. Serum vasoconstrictor, serotonin; isolation and characterization. J Biol Chem. 1948; 176:1243–1251. [PubMed: 18100415]
3. Blackburn KJ, French PC, Merrills RJ. 5-hydroxytryptamine uptake by rat brain in vitro. Life Sci. 1967; 6:1653–1663. [PubMed: 5299290]
4. Carlsson A, Fuxe K, Ungerstedt U. The effect of imipramine on central 5-hydroxytryptamine neurons. J Pharm Pharmacol. 1968; 20:150–151. [PubMed: 4384540]
5. Glowinski J, Axelrod J. Inhibition of uptake of tritiated-noradrenaline in the intact rat brain by imipramine and structurally related compounds. Nature. 1964; 204:1318–1319. [PubMed: 14254430]
6. Hoffman BJ, Mezey E, Brownstein MJ. Cloning of a serotonin transporter affected by antidepressants. Science. 1991; 254:579–580. [PubMed: 1948036]
7. Blakely RD, et al. Cloning and expression of a functional serotonin transporter from rat brain. Nature. 1991; 354:66–70. [PubMed: 1944572]
8. Kristensen AS, et al. SLC6 neurotransmitter transporters: structure, function, and regulation. Pharmacol Rev. 2011; 63:585–640. [PubMed: 21752877]
9. Broer S, Gether U. The solute carrier 6 family of transporters. Br J Pharmacol. 2012; 167:256–278. [PubMed: 22519513]
10. Wennogle LP, Meyerson LR. Serotonin modulates the dissociation of [3H]imipramine from human platelet recognition sites. Eur J Pharmacol. 1982; 86:303–307. [PubMed: 7160439]
11. Zhong H, et al. An allosteric binding site at the human serotonin transporter mediates the inhibition of escitalopram by R-citalopram: kinetic binding studies with the ALI/VFL-SI/TT mutant. Neurosci Lett. 2009; 462:207–212. [PubMed: 19616061]
12. Hahn MK, Blakely RD. The functional impact of SLC6 transporter genetic variation. Annu Rev Pharmacol Toxicol. 2007; 47:401–441. [PubMed: 17067279]
13. Andersen J, Kristensen AS, Bang-Andersen B, Stromgaard K. Recent advances in the understanding of the interaction of antidepressant drugs with serotonin and norepinephrine transporters. Chem Commun (Camb). 2009:3677–3692. [PubMed: 19557250]
14. Singh SK, Piscitelli CL, Yamashita A, Gouaux E. A competitive inhibitor traps LeuT in an open-to-out conformation. Science. 2008; 322:1655–1661. [PubMed: 19074341]
15. Wang H, et al. Structural basis for action by diverse antidepressants on biogenic amine transporters. Nature. 2013; 503:141–145. [PubMed: 24121440]
16. Yamashita A, Singh SK, Kawate T, Jin Y, Gouaux E. Crystal structure of a bacterial homologue of Na+/Cl--dependent neurotransmitter transporters. Nature. 2005; 437:215–223. [PubMed: 16041361]

17. Singh SK, Pal A. Biophysical approaches to the study of LeuT, a prokaryotic homolog of neurotransmitter sodium symporters. Methods Enzymol. 2015; 557:167–198. [PubMed: 25950965]
18. Kazmier K, et al. Conformational dynamics of ligand-dependent alternating access in LeuT. Nat Struct Mol Biol. 2014; 21:472–479. [PubMed: 24747939]
19. Wang KH, Penmatsa A, Gouaux E. Neurotransmitter and psychostimulant recognition by the dopamine transporter. Nature. 2015; 521:322–327. [PubMed: 25970245]
20. Penmatsa A, Wang KH, Gouaux E. X-ray structures of Drosophila dopamine transporter in complex with nisoxetine and reboxetine. Nat Struct Mol Biol. 2015; 22:506–508. [PubMed: 25961798]
21. Penmatsa A, Wang KH, Gouaux E. X-ray structure of dopamine transporter elucidates antidepressant mechanism. Nature. 2013; 503:85–90. [PubMed: 24037379]
22. Ramamoorthy S, et al. Antidepressant- and cocaine-sensitive human serotonin transporter: molecular cloning, expression, and chromosomal localization. Proc Natl Acad Sci U S A. 1993; 90:2542–2546. [PubMed: 7681602]
23. Green EM, Coleman JA, Gouaux E. Thermostabilization of the human serotonin transporter in an antidepressant-Bound Conformation. Plos One. 2015; 10:e0145688. [PubMed: 26695939]
24. Kawate T, Gouaux E. Fluorescence-detection size-exclusion chromatography for precrystallization screening of integral membrane proteins. Structure. 2006; 14:673–681. [PubMed: 16615909]
25. Goehring A, et al. Screening and large-scale expression of membrane proteins in mammalian cells for structural studies. Nat Protoc. 2014; 9:2574–2585. [PubMed: 25299155]
26. Krishnamurthy H, Gouaux E. X-ray structures of LeuT in substrate-free outward-open and apo inward-open states. Nature. 2012; 481:469–474. [PubMed: 22230955]
27. Chen JG, Liu-Chen S, Rudnick G. External cysteine residues in the serotonin transporter. Biochemistry. 1997; 36:1479–1486. [PubMed: 9063896]
28. Tate CG, Blakely RD. The effect of N-linked glycosylation on activity of the Na(+)- and Cl(−)-dependent serotonin transporter expressed using recombinant baculovirus in insect cells. J Biol Chem. 1994; 269:26303–26310. [PubMed: 7523405]
29. Kilic F, Rudnick G. Oligomerization of serotonin transporter and its functional consequences. Proc Natl Acad Sci U S A. 2000; 97:3106–3111. [PubMed: 10716733]
30. Rasmussen TN, Plenge P, Bay T, Egebjerg J, Gether U. A single nucleotide polymorphism in the human serotonin transporter introduces a new site for N-linked glycosylation. Neuropharmacology. 2009; 57:287–294. [PubMed: 19500602]
31. Owens MJ, Knight DL, Nemeroff CB. Second-generation SSRIs: human monoamine transporter binding profile of escitalopram and R-fluoxetine. Biol Psychiatry. 2001; 50:345–350. [PubMed: 11543737]
32. Andersen J, et al. Mutational mapping and modeling of the binding site for (S)-citalopram in the human serotonin transporter. J Biol Chem. 2010; 285:2051–2063. [PubMed: 19892699]
33. Koldso H, et al. The two enantiomers of citalopram bind to the human serotonin transporter in reversed orientations. J Am Chem Soc. 2010; 132:1311–1322. [PubMed: 20055463]
34. Sorensen L, et al. Interaction of antidepressants with the serotonin and norepinephrine transporters: mutational studies of the S1 substrate binding pocket. J Biol Chem. 2012; 287:43694–43707. [PubMed: 23086945]
35. Barker EL, et al. High affinity recognition of serotonin transporter antagonists defined by species-scanning mutagenesis. An aromatic residue in transmembrane domain I dictates species-selective recognition of citalopram and mazindol. J Biol Chem. 1998; 273:19459–19468. [PubMed: 9677366]
36. Forrest LR, Tavoulari S, Zhang YW, Rudnick G, Honig B. Identification of a chloride ion binding site in Na+/Cl -dependent transporters. Proc Natl Acad Sci U S A. 2007; 104:12761–12766. [PubMed: 17652169]
37. Kantcheva AK, et al. Chloride binding site of neurotransmitter sodium symporters. Proc Natl Acad Sci U S A. 2013; 110:8489–8494. [PubMed: 23641004]
38. Humphreys CJ, Wall SC, Rudnick G. Ligand binding to the serotonin transporter: equilibria, kinetics, and ion dependence. Biochemistry. 1994; 33:9118–9125. [PubMed: 8049215]

39. Andersen J, et al. Molecular determinants for selective recognition of antidepressants in the human serotonin and norepinephrine transporters. Proc Natl Acad Sci U S A. 2011; 108:12137–12142. [PubMed: 21730142]
40. Henry LK, et al. Tyr-95 and Ile-172 in transmembrane segments 1 and 3 of human serotonin transporters interact to establish high affinity recognition of antidepressants. J Biol Chem. 2006; 281:2012–2023. [PubMed: 16272152]
41. Tavoulari S, Forrest LR, Rudnick G. Fluoxetine (Prozac) binding to serotonin transporter is modulated by chloride and conformational changes. J Neurosci. 2009; 29:9635–9643. [PubMed: 19641126]
42. Zheng H, Chruszcz M, Lasota P, Lebioda L, Minor W. Data mining of metal ion environments present in protein structures. J Inorg Biochem. 2008; 102:1765–1776. [PubMed: 18614239]
43. Singh SK, Yamashita A, Gouaux E. Antidepressant binding site in a bacterial homologue of neurotransmitter transporters. Nature. 2007; 448:952–956. [PubMed: 17687333]
44. Zhou Z, et al. LeuT-desipramine structure reveals how antidepressants block neurotransmitter reuptake. Science. 2007; 317:1390–1393. [PubMed: 17690258]
45. Zhou Z, et al. Antidepressant specificity of serotonin transporter suggested by three LeuT-SSRI structures. Nat Struct Mol Biol. 2009; 16:652–657. [PubMed: 19430461]
46. Plenge P, et al. Steric hindrance mutagenesis in the conserved extracellular vestibule impedes allosteric binding of antidepressants to the serotonin transporter. J Biol Chem. 2012; 287:39316–39326. [PubMed: 23007398]
47. Jacobsen JP, et al. The interaction of escitalopram and R-citalopram at the human serotonin transporter investigated in the mouse. Psychopharmacology (Berl). 2014; 231:4527–4540. [PubMed: 24810106]
48. Scanlon SM, Williams DC, Schloss P. Membrane cholesterol modulates serotonin transporter activity. Biochemistry. 2001; 40:10507–10513. [PubMed: 11523992]
49. Koban F, et al. A salt bridge linking the first intracellular loop with the C terminus facilitates the folding of the serotonin transporter. J Biol Chem. 2015; 290:13263–13278. [PubMed: 25869136]
50. Sucic S, et al. Switching the clientele: a lysine residing in the C terminus of the serotonin transporter specifies its preference for the coat protein complex II component SEC24C. J Biol Chem. 2013; 288:5330–5341. [PubMed: 23288844]
51. Galfre G, Howe SC, Milstein C, Butcher GW, Howard JC. Antibodies to major histocompatibility antigens produced by hybrid cell lines. Nature. 1977; 266:550–552. [PubMed: 558524]
52. Reeves PJ, Callewaert N, Contreras R, Khorana HG. Structure and function in rhodopsin: high-level expression of rhodopsin with restricted and homogeneous N-glycosylation by a tetracycline-inducible N-acetylglucosaminyltransferase I-negative HEK293S stable mammalian cell line. Proc Natl Acad Sci U S A. 2002; 99:13419–13424. [PubMed: 12370423]
53. Kabsch W. Xds. Acta Crystallogr D Biol Crystallogr. 2010; 66:125–132. [PubMed: 20124692]
54. Afonine PV, et al. Towards automated crystallographic structure refinement with phenix.refine. Acta Crystallogr D Biol Crystallogr. 2012; 68:352–367. [PubMed: 22505256]
55. Bunkoczi G, et al. Phaser. MRage: automated molecular replacement. Acta Crystallogr D Biol Crystallogr. 2013; 69:2276–2286. [PubMed: 24189240]
56. McCoy AJ, et al. Phaser crystallographic software. J Appl Crystallogr. 2007; 40:658–674. [PubMed: 19461840]
57. Hanson MA, et al. Crystal structure of a lipid G protein-coupled receptor. Science. 2012; 335:851–855. [PubMed: 22344443]
58. Sali A, Blundell TL. Comparative protein modelling by satisfaction of spatial restraints. J Mol Biol. 1993; 234:779–815. [PubMed: 8254673]
59. Kyte J, Doolittle RF. A simple method for displaying the hydropathic character of a protein. J Mol Biol. 1982; 157:105–132. [PubMed: 7108955]

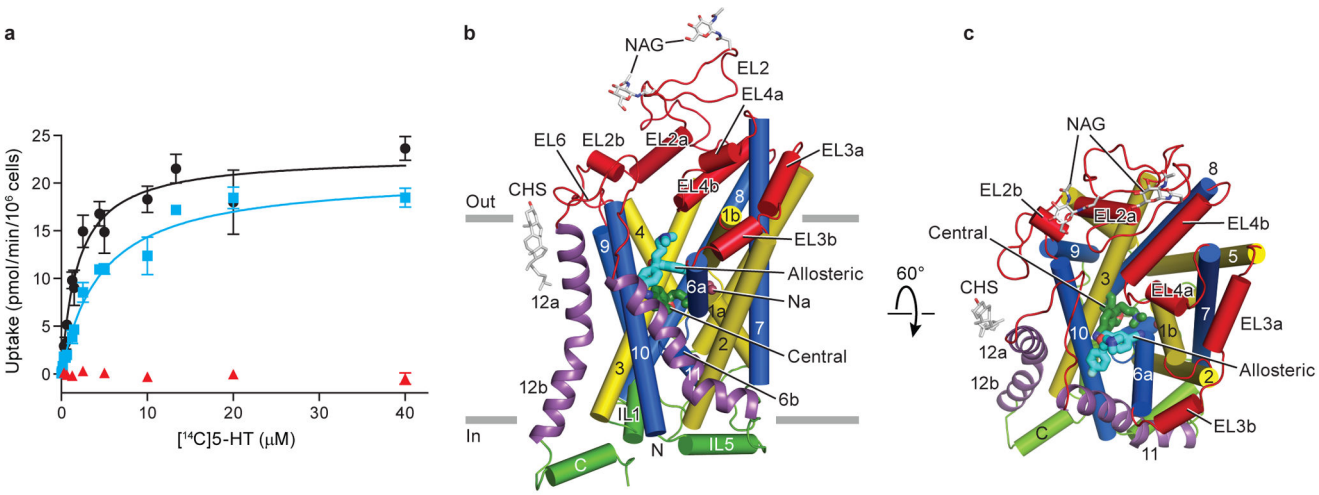


**Figure 1. Function and architecture of the human serotonin transporter**

**a**, Michaelis-Menten plots of serotonin (5-HT) uptake by wild-type (black, circles), ts2 (blue, squares), and ts3 (red, triangles) transporters. Graph depicts an average of three independent experiments, each performed with triplicate measurements (error bars represent s.e.m.). **b**, Structure of SERT viewed parallel to the membrane. (*S*)-citalopram molecules (central) and (allosteric) are shown as sticks in dark green and cyan, respectively. Sodium ions are shown as spheres in salmon. Cholesteryl hemisuccinate (CHS) and *N*-acetylglucosamine (NAG) are shown as sticks. **c**, View of SERT from the extracellular side of the membrane.

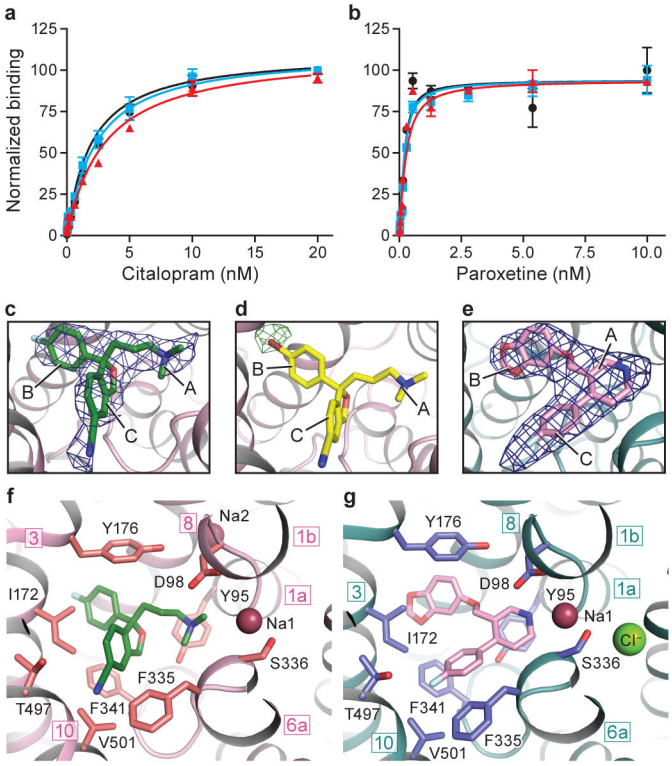


**Figure 2. Antidepressant binding and recognition**

**a**, Graph of [$^3$H](*R/S*)-citalopram saturation binding to wild-type (black, circles), ts2 (blue, squares), and ts3 (red, triangles) transporters, showing the average of two independent experiments, each performed in triplicate (error bars represent s.e.m.). **b**, Plot of a [$^3$H]-paroxetine saturation binding from a representative experiment (error bars represent s.e.m. from triplicate measurements). **c**, $F_o$-$F_c$ omit (*S*)-citalopram electron density (blue mesh), contoured at 3σ. The approximate positions of subsites A, B, C are shown. **d**, Anomalous difference electron density (green mesh), derived from Br-citalopram (yellow sticks) bound to the central site is shown (8.0σ contour level). **e**, $F_o$-$F_c$ omit electron density for paroxetine, contoured at 3σ. **f**, Interactions of (*S*)-citalopram (dark green) in the central binding site. **g**, Interactions of paroxetine (pink) with residues in the central binding site.

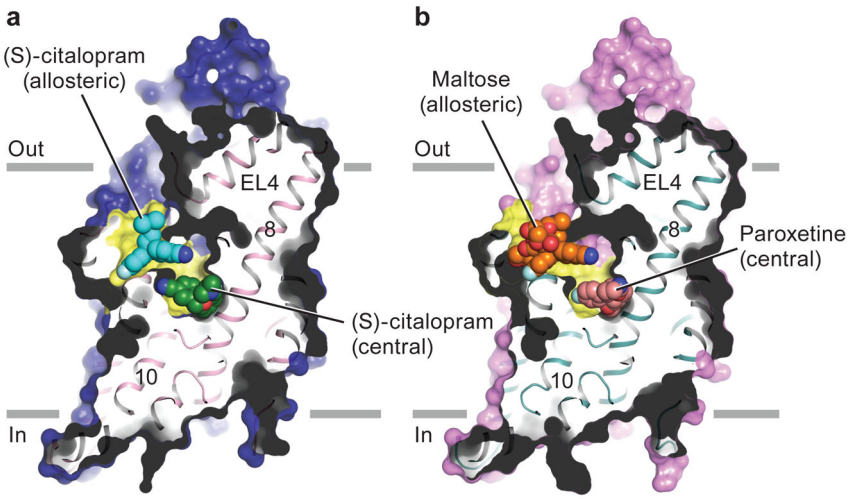


**Figure 3. Allosteric site**

**a**, Sagittal slice through a surface representation of the (*S*)-citalopram-bound transporter. (*S*)-citalopram molecules bound to the allosteric (cyan) and central (green) sites are shown as spheres. **b**, A maltose headgroup (orange), derived from a detergent molecule and bound to the allosteric site, and paroxetine (pink), bound to the central site, are shown as spheres.

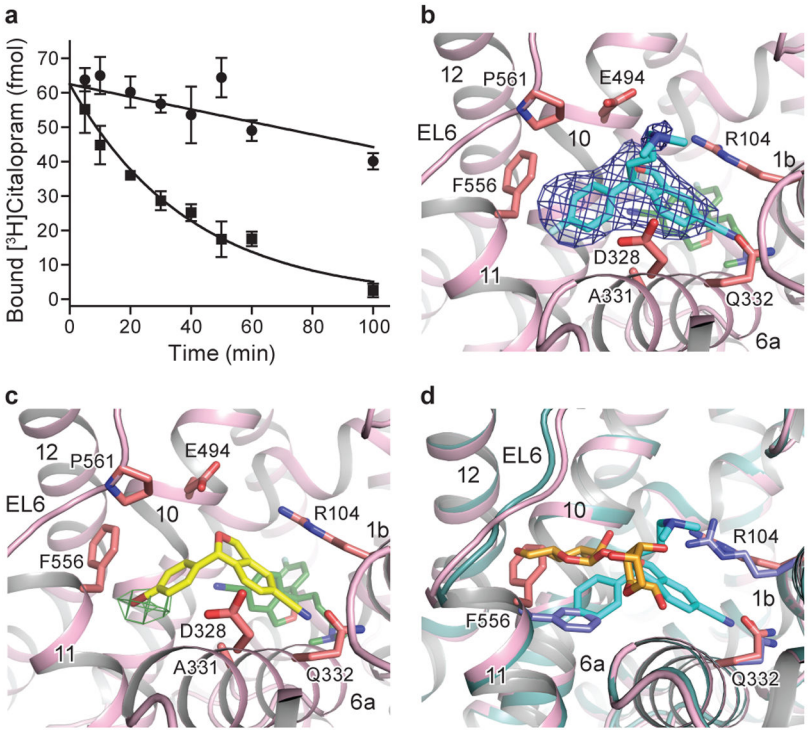


**Figure 4. Structural basis of allosteric regulation**

**a**, Dissociation of [$^3$H](*R/S*)-citalopram in the presence of buffer containing 100 μM (*S*)-citalopram (circles) or without ligand (squares). A representative experiment is shown (error bars represent s.e.m. from triplicate measurements). **b**, Allosteric site bound with (*S*)-citalopram (cyan). Residues in close proximity to (*S*)-citalopram are shown as sticks. A few atoms of (*S*)-citalopram at the central site (green sticks) are visible 'below' the (*S*)-citalopram molecule bound to the allosteric site. $F_o$-$F_c$ omit density of (*S*)-citalopram (blue mesh) in the allosteric site is shown (1.5σ contour level). **c**, Anomalous difference electron density (green mesh), derived from a Br-citalopram (yellow sticks) diffraction data set, is contoured at 5σ. **d**, Alignment of the allosteric site of the paroxetine (blue) and (*S*)-citalopram-bound (pink) structures. Maltose is in orange sticks. Superposition was performed over all Cα atoms of the transporter.

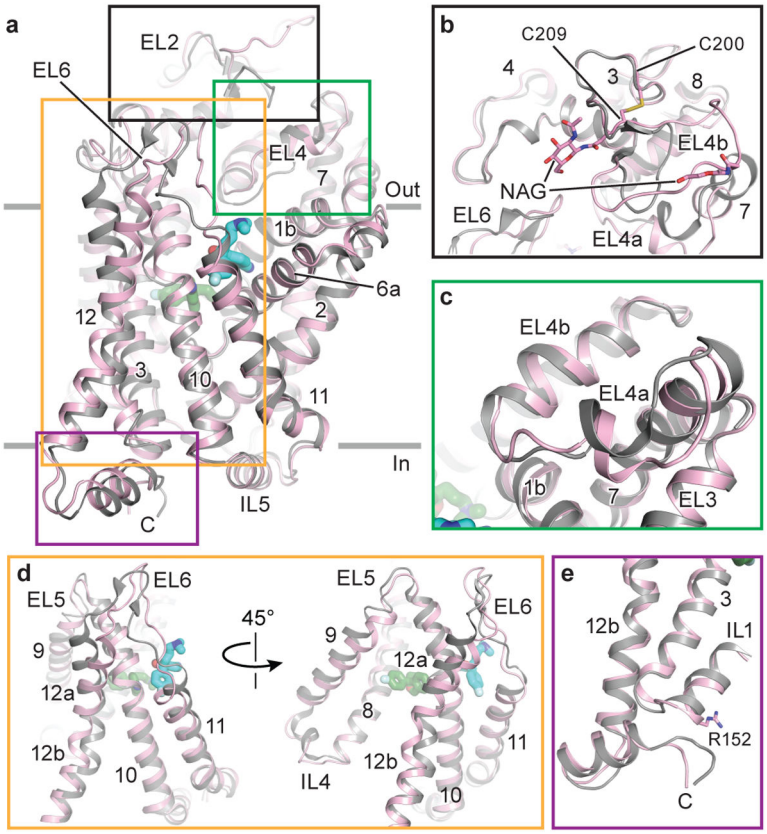


**Figure 5. Comparison of serotonin and dopamine transporters**

**a**, Overall alignment of SERT (pink) *vs.* dDAT (grey) using TMs 1–12; regions in SERT with structural differences are boxed. (*S*)-citalopram bound to the central (green) and allosteric (cyan) sites shown as sticks. **b**, Close up view of EL2, *N*-acetylglucosamine (NAG; SERT) and the disulfide bridge between C200 and C209 are shown as sticks. **c**, View of EL4. **d**, Structural differences at the SERT allosteric site showing TMs 9, 10, 11, 12, EL6, and IL4. **e**, Conformation of the C-terminal helix and IL1. R152 of SERT is in sticks.

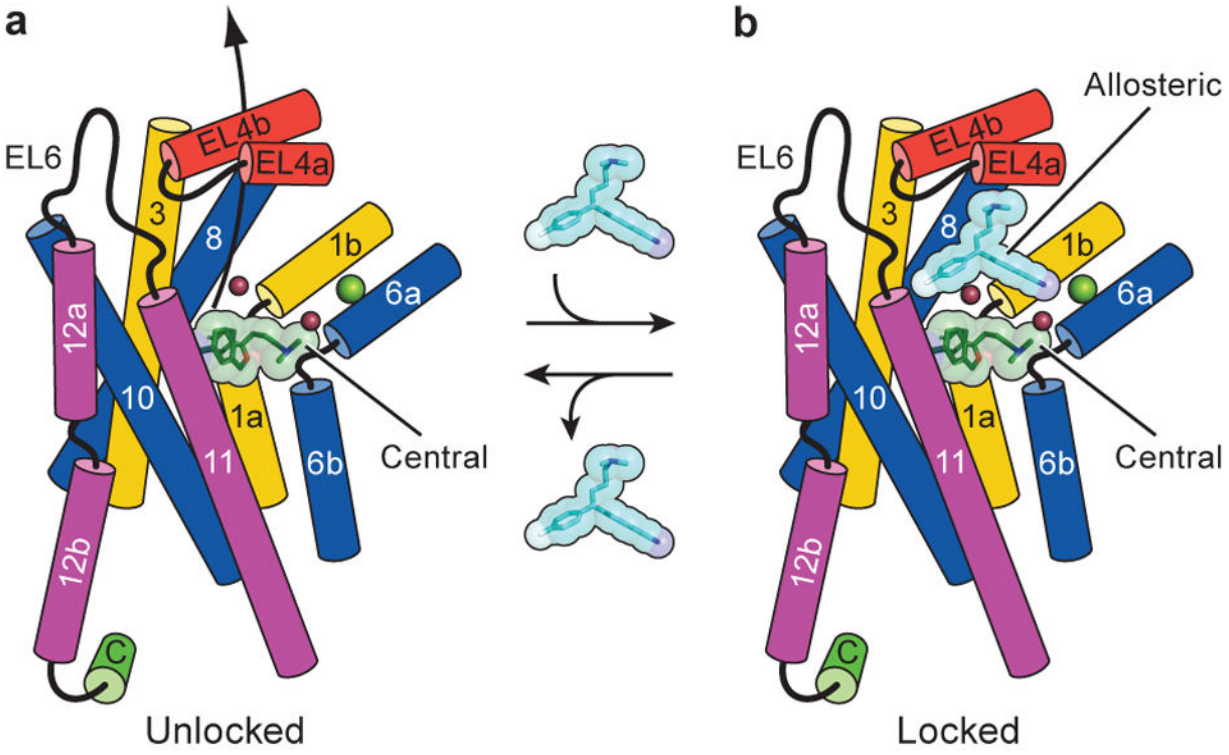


**Figure 6. Allosteric modulation of inhibitor binding**

**a**, The SSRI (*S*)-citalopram (dark green) binds to the central site by wedging between scaffold helices 3, 8, and 10 and core helices 1 and 6. Sodium and chloride ions are shown as salmon and green spheres. **b**, (*S*)-citalopram (cyan) binds to the allosteric site made up of TMs 1b, 6a, 10, 11, EL4, and EL6. Binding to the allosteric site prevents dissociation from the central site.